Monthly Notices
of the
ROYAL ASTRONOMICAL SOCIETY

MNRAS **491,** 264–271 (2020)
Advance Access publication 2019 October 31

doi:10.1093/mnras/stz3035

An empirical fit for viscoelastic simulations of tertiary tides

Yan Gao,[1,2,3]★ Silvia Toonen,[4,5] Evgeni Grishin,[6] Tom Comerford[7] and Matthias U. Kruckow[1,2]

[1]*Yunnan Observatories, Chinese Academy of Sciences, Kunming 650011, China*
[2]*Key Laboratory for the Structure and Evolution of Celestial Objects, Chinese Academy of Sciences, Kunming 650011, China*
[3]*University of Chinese Academy of Sciences, No.19(A) Yuquan Road, Shijingshan District, Beijing 100049, P.R.China*
[4]*Anton Pannekoek Institute for Astronomy, University of Amsterdam, NL-1090 GE Amsterdam, the Netherlands*
[5]*Institute for Gravitational Wave Astronomy, School of Physics and Astronomy, University of Birmingham, Birmingham B15 2TT, UK*
[6]*Physics Department, Technion – Israel Institute of Technology, Haifa 3200003, Israel*
[7]*Institute of Astronomy, University of Cambridge, Madingley Road, Cambridge CB3 0HA, UK*

Accepted 2019 October 24. Received 2019 October 24; in original form 2019 August 24

ABSTRACT

Tertiary tides (TTs), or the continuous tidal distortion of the tertiary in a hierarchical triple system, can extract energy from the inner binary, inducing within it a proclivity to merge. Despite previous work on the subject, which established that it is significant for certain close triple systems, it is still not a well-understood process. A portion of our ignorance in this regard stems from our inability to integrate a simulation of this phenomenon into conventional stellar evolution codes, since full calculations of these tidal interactions are computationally expensive on stellar evolution time-scales. Thus, to attain a better understanding of how these TTs act on longer time-scales, an empirical expression of its effects as a function of parameters of the triple system involved is required. In this work, we evaluate the rate at which TTs extract energy from the inner binary within a series of constructed hierarchical triple systems under varying parameters, and study the rate at which the inner binary orbital separation shrinks as a function of those parameters. We find that this rate varies little with the absolute values of the masses of the three component objects, but is very sensitive to the mass ratio of the inner binary q, the tertiary radius R_3, the inner binary orbital separation a_1, the outer orbital separation a_2, and the viscoelastic relaxation time of the tertiary τ. More specifically, we find that the percentage by which a_1 shrinks per unit time can be reasonably approximated by $(1/a_1)(\mathrm{d}a_1/\mathrm{d}t) = (2.22 \times 10^{-8}\ \mathrm{yr}^{-1})4q(1+q)^{-2}(R_3/100\ \mathrm{R}_\odot)^{5.2}(a_1/0.2\ \mathrm{au})^{4.8}(a_2/2\ \mathrm{au})^{-10.2}(\tau/0.534\ \mathrm{yr})^{-1.0}$. We also provide tests of how precise this fitting function is.

Key words: celestial mechanics – binaries: close – stars: evolution.

1 INTRODUCTION

Previous studies (Gao et al. 2018, henceforth GCEH18; see also Fuller et al. 2013) have established the fact that in a hierarchical triple system where the tertiary is sufficiently close to the inner binary, it extracts orbital energy from the inner binary via purely tidal interactions, giving rise within the inner binary a proclivity to merge. These tidal interactions are known as tertiary tides, or TTs for short. Since this merging process and its subsequent influence on the evolution of the triple system happen on time-scales comparable to typical stellar evolution time-scales, it would be desirable to integrate this process into a stellar evolution code. However, as the tidal effects leading to this merging process occur on time-scales much shorter than stellar evolution time-scales, it would be impractical to run a simulation of these tidal effects in parallel with a stellar evolution code. This complication is further compounded by the fact that triple evolution codes already need to deal with a host of complicated processes not seen in binaries, more of which are being discovered every year (e.g. Di Stefano 2019). The conventional way around such a problem would be to perform a set of simulations for a grid of parameters, so that detailed calculations can be replaced by interpolations and/or extrapolations of the aforementioned grid (e.g. Hurley, Pols & Tout 2000; Hurley, Tout & Pols 2002; Dotter 2016), which can then be implemented in stellar evolution codes with relative ease. But since no such grid has yet been simulated for TTs, doing so would seem to be a natural course of action, hence this paper.

Since, in our previous studies, we found that the main influence of TTs is to quickly shrink the inner orbit of its host hierarchical

★ E-mail: ygbcyy@ynao.ac.cn

triple, the speed at which this happens will be the main focus of this work. Ideally, we wish to obtain da_1/dt as a function of the orbital parameters of the hierarchical triple, so that any triple stellar evolution code (e.g. Toonen, Hamers & Portegies Zwart 2017) can easily implement this during the course of integrating the relevant stellar evolution functions, with little extra expenditure in terms of computing time. This function is therefore what we will aim to calculate empirically using our grid of simulations. Other effects, such as the seemingly negligible excitation of eccentricities of the inner and outer orbits, which may or may not be important, are still not well understood, and in any case do not affect the host triple system as obviously as the orbital shrinkage, so we leave them to future studies.

In this paper, we use our previous models to calculate the energy extraction rate for triples with varying orbital parameters, and provide an empirical fit to the results, thereby establishing the desired empirical function. In Section 2, we present our models and methods for calculating this energy extraction rate for individual systems. In Section 3, we display our results and our empirical fits to the results, and finally we discuss the implications of our work in Section 4.

2 METHODS

2.1 Simulations of tertiary tides

To simulate a close hierarchical triple system undergoing TTs, we refer to our previous methods used in GCEH18. In that paper, the simulation is carried out in two stages. In the first stage, we used a lagged equilibrium tidal model (Hut 1981; Eggleton, Kiseleva & Hut 1998; Kiseleva, Eggleton & Mikkola 1998; Correia, Boué & Laskar 2016) to estimate the magnitude of the rate of energy extraction under a set of assumptions. We then move on to the second stage, which uses a viscoelastic tidal model (Correia & Rodríguez 2013; Correia et al. 2014), in which there is an unknown parameter τ. We calibrate this τ by varying it until the resulting energy extraction rate matches that obtained in the first stage. The rationale for conducting such a two-step simulation is that the two stages overcome each other's shortcomings: the assumptions made for constructing the equilibrium tidal model are rigid and extreme, including demanding that the inner binary components are of equal mass, and work only for very special hierarchical triple systems, as well as making a host of approximations that may undermine its accuracy regarding the finer details; the viscoelastic model, on the other hand, suffers from no such problems, but has the aforementioned unknown parameter τ, for which there is no established method of calculating through first principles.

For our following work simulating a set of hierarchical triples under varying parameters, we opt to use the second stage only, leaving τ as a free parameter in our final empirical fit. This decision is due to the fact that the first-stage simulations previously conducted operate under assumptions that break down for much of the parameter space over which we vary, notably for different values of m_1 and m_2.

As a starting point for our following investigation, we revert to our hypothetical scenario previously presented in GCEH18. The initial parameters of this system are presented in Table 1, where a_1 and a_2 are, respectively, the semimajor axes of the inner and outer orbits, e_1 and e_2 are the eccentricities of the inner and outer orbits, i is the inclination angle between the two orbits, m_1 and m_2 are the masses of the inner binary, m_3 is the mass of the tertiary, R_3 is the radius of the tertiary, and τ is the viscoelastic relaxation time

Table 1. Initial parameters for our simulations, both for the hypothetical scenario that we use as a starting point and the range of values that each parameter was varied over.

Parameter	Hypothetical scenario	Range varied over
a_1 (au)	0.2	0.04–0.4
a_2 (au)	2.0	2.0–3.8
e_1	0	–
e_2	0	–
i	0	–
m_1 ($M_\odot$)	0.8	0.15–1.5
m_2 ($M_\odot$)	0.8	See text
m_3 ($M_\odot$)	1.6	0.2–1.6
R_3 ($R_\odot$)	100	20–200
τ (yr)	0.534	0.1–1

mentioned above. When simulating this system, we select initial positions such that the vectors for a_1 and a_2 are perpendicular to each other, and initial velocities for each of the bodies such that all orbits are circular and coplanar. We simulate the system's tidal evolution for 10^5 yr, during which the shrinkage of the inner binary's orbit behaves linearly.

We then proceed to vary the parameters m_1, $q = m_1/m_2$, m_3, R_3, τ, a_1, and a_2 one by one, while keeping the other parameters constant, and performing the same simulation. The ranges over which we vary these parameters are also presented in Table 1. This results in a set of energy extraction rates for different parameters, to which we then perform the desired empirical fit. While not, strictly speaking, a grid of simulations in parameter space, this set of simulations will prove insightful, as demonstrated below.

To speed up our calculations, we translate our original simulation code from eighth-order Runge–Kutta to a variable steplength Bulirsch–Stoer algorithm, which costs only a tenth of the calculation time of the original implementation used in GCEH18. We check the consistency of the two codes by repeating our previous simulation runs using our new code, the results of which we find to be practically identical to our original ones.

2.2 Calculation of energy extraction rate from the inner binary

As seen in GCEH18, the magnitude of the inner binary orbital separation oscillates as it shrinks, leading to an inner binary orbital energy value that is constantly oscillating as it becomes smaller. A typical example of this is shown in Fig. 1. For the simulations conducted in GCEH18, the amount by which the inner orbit shrinks is so much that this oscillation becomes little more than an insignificant background noise. However, in the simulations below, the inner binary orbital shrinkage is comparable in magnitude or even smaller than this oscillation over the simulated period of 10^5 yr in many instances. Consequently, we cannot simply compare the initial and final inner orbital energies at the beginning and end of the simulation to obtain the energy extraction rate as we did previously. To overcome this oscillation, we take the initial inner binary orbital energy to be that at the first minimum that occurs in our a_1, and the final inner binary orbital energy to be that at the last minimum. It is the difference between these two values that we use for the amount of energy extracted. It should be noted here that we also checked the corresponding values calculated using the first and last maxima instead of the minima, as well as the average of the two, and find no significant difference between the results. The fact that we use minima is just an arbitrary preference.

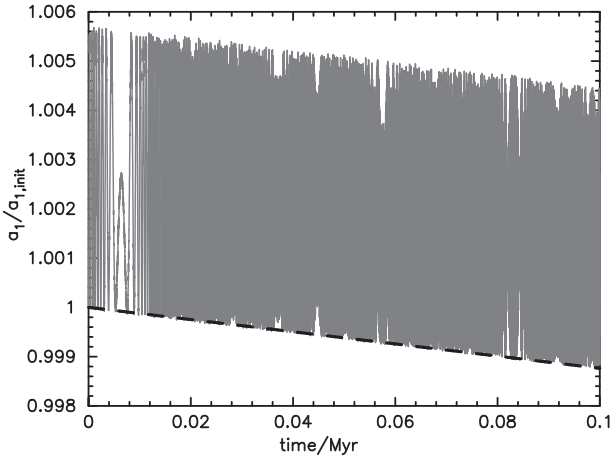

Figure 1. Typical example of the oscillatory evolution of the inner binary orbital separation under the influence of tertiary tides. The apparent beating pattern is not a physical phenomenon, but is rather due to Nyquist frequency (aliasing) issues introduced by the plotting process. The dashed line, which traces the positions of the minima of this oscillation, is plotted by connecting the lowest minimum among the first 10 minima, and the lowest minimum among the last 10 minima of this oscillation. In our subsequent plots, we use this method to plot the evolution of these minima values, since the resulting line is aesthetically identical to the actual evolution curves of these minima.

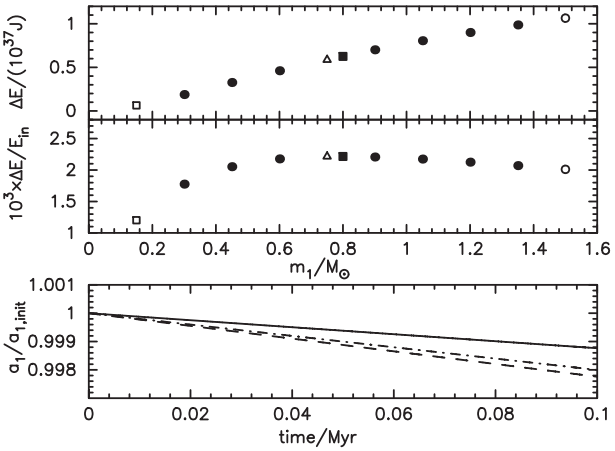

Figure 2. Starting with the hypothetical system described in Table 1 (represented by the filled square), m_1 is varied while keeping all other parameters constant. Plotted are the results of 10 simulation runs, each for 10^5 yr. Plotted in the upper panel is the amount of energy extracted from the inner binary in each run as a function of m_1. Plotted in the upper half of the upper panel is the absolute amount of energy extracted within those 10^5 yr (ΔE), while the lower half of the upper panel depicts this ΔE in terms of the ratio $\Delta E/E_{\rm in}$, where $E_{\rm in}$ is the total orbital energy of the inner binary at the beginning of the simulation (at the beginning of those 10^5 yr). The lower panel plots the evolution of the minima values of each oscillation of the inner binary orbital semimajor axis for some of the models in the upper panel. The solid, dashed, and dash–dotted lines correspond to the models represented by the non-filled square, triangle, and circle in the upper panel, respectively.

To estimate the precision of our simulations, we set the tertiary radius to progressively smaller values in the hypothetical scenario listed in Table 1, at some point of which TTs ought to become so insignificant that the apparent amount of energy extracted is dominated by the intrinsic errors of our method. We then take the noise level recovered in this way to be the errors of our simulations. This noise level was found to be 2×10^{33} J over a simulation of 10^5 yr.

3 RESULTS

In this section, we will present the amount of energy extracted from the inner binary in a set of simulations where the parameters of the triple system are varied. The orbital energy is connected to the inner binary orbital separation by

$$a_1 \propto -\frac{1}{E_{\rm in}}, \tag{1}$$

where a_1 is the inner binary orbital separation, and $E_{\rm in}$ in the inner binary orbital energy (note that it is always smaller than zero). For constant values of m_1, m_2, and m_3 during the course of evolution, assuming small $\mathrm{d}a_1$ and $\mathrm{d}E_{\rm in}$, we have the approximation

$$\frac{\mathrm{d}a_1}{a_1} = \frac{\mathrm{d}E_{\rm in}}{E_{\rm in}}. \tag{2}$$

Therefore, for the simulation runs mentioned in this paper, we will be presenting the amount of energy extracted from the inner binary in terms of $\Delta E/E_{\rm in}$, which is also a proxy for the amount by which the inner binary orbital separation has shrunk.

3.1 Influence of inner binary masses

First of all, we set all the parameters to be equal to those of the hypothetical scenario detailed in Table 1, with the exception of m_1, which we vary from 0.15 to 1.5 $M_\odot$. For each value of m_1, we run the simulation for 10^5 yr, during which the inner binary orbital shrinkage is small and behaves linearly, and we expect equation (2) to hold. The results of these simulations are presented in Fig. 2, where it can be seen that $\Delta E/E_{\rm in}$, and hence the orbital shrinkage, peaks at around $m_1 = m_2$. The result of the hypothetical scenario listed in Table 1, where m_1 is actually equal to m_2, is also plotted for comparison. We also test the validity of equation (2) by plotting the evolution of the minima of a_1 as a function of time, which should provide a straightforward idea of how fast the inner binary orbit actually shrinks. This evolution behaves as expected.

So, what if the total inner binary mass remains constant, but the mass ratio $q = m_1/m_2$ varies? Varying q between 0.1 and 1 while keeping $m_1 + m_2$ constant at 1.6 $M_\odot$, we arrive at Fig. 3, where it can be seen that the energy extraction rate decays slowly as q approaches 0. This is to be expected, as the gravitational potential variation at the tertiary due to the inner binary orbit decreases with smaller q.

Next, we set q to be constant at 1, but vary m_1, and the result is plotted in Fig. 4. It appears that $\Delta E/E_{\rm in}$ changes little, regardless of what masses are given for the inner binary, as long as $q = 1$.

Comparing Figs 2–4, it is apparent that the maximum value for $\Delta E/E_{\rm in}$ is achieved when q is about equal to 1, and that this maximum value does not change much with the values of m_1 and m_2. So do the values of m_1 and m_2 matter at all, given that q remains the same? To check this, we again vary q while keeping $m_1 + m_2$ constant at 1.6 $M_\odot$, but this time we set q to exactly the same values inadvertently obtained in Fig. 2, where we varied m_1 while keeping m_2 constant. The results of this set of simulations are displayed in Fig. 5, plotted over the results shown in Fig. 2. Indeed, it can be seen that $\Delta E/E_{\rm in}$ is insensitive to the absolute values of the inner binary masses, as long as q remains the same.

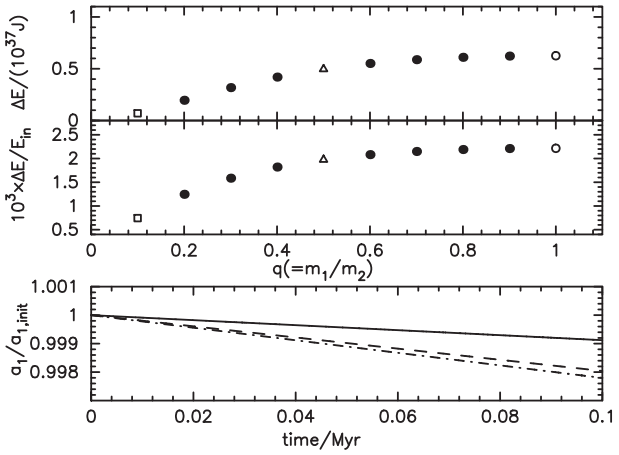

Figure 3. Similar to the previous plot, only this time $m_1 + m_2$ was kept constant, and the mass ratio $q = m_1/m_2$ is varied. All other parameters are kept constant and equal to the hypothetical system described in Table 1. The meaning of the panels, symbols, and line styles are the same as those in Fig. 2.

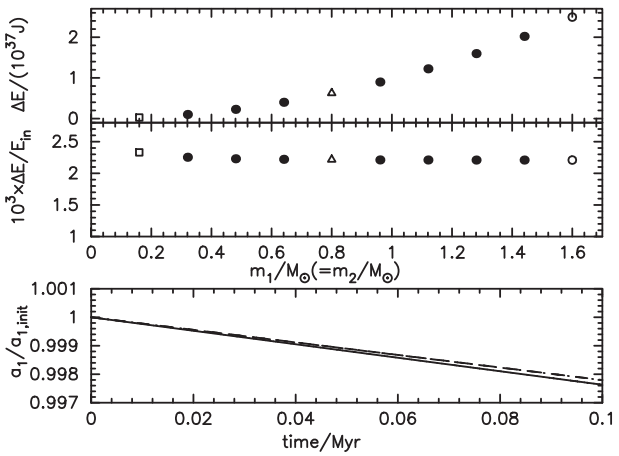

Figure 4. In this figure, q is kept constant at 1, while the total value of $m_1 + m_2$ is varied. All other parameters are kept constant and equal to the hypothetical system described in Table 1. The meaning of the panels, symbols, and line styles are the same as those in Fig. 2.

Why is this the case? To answer this question, we refer to the calculations done in appendix A of GCEH18, culminating in their equation (A14), repeated below:

$$\Delta E_{\rm P} \sim \frac{135}{4}\frac{Gm^2R_3^5a_1^2}{a_2^8}, \tag{3}$$

where $E_{\rm P}$ is the greatest self-gravitational potential difference that m_3 can undergo, assuming that it is always at equilibrium tide, G is the gravitational constant, and $m = m_1 = m_2$ (the equation was derived under the assumption that $m_1 = m_2$). While $E_{\rm P}$ has little to do with the actual energy extraction rate (the two are only equivalent if m_3 is constantly at equilibrium tide and tidal dissipation is infinitely efficient, neither of which is ever the case), it does decree the absolute upper limit that can be extracted within 1/4 of an inner binary orbit, and thus this expression provides some interesting insights as to how the gravitational field difference at m_3 scales with the inner masses. As in the equation, the capability of the inner binary to distort the tertiary scales proportionally with m^2, while the energy required to shrink a_1 by a certain factor is also proportional

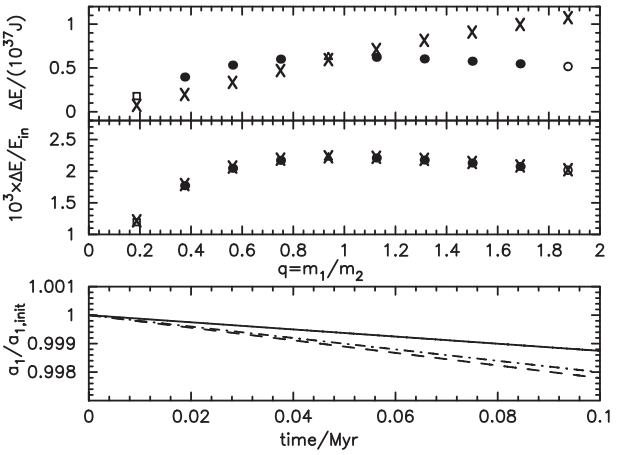

Figure 5. Keeping $m_1 + m_2$ constant at 1.6 $M_\odot$, q is varied to match the mass ratios induced by varying m_1 in Fig. 2. The data points from Fig. 2 are plotted over these results as crosses. The meaning of the panels, symbols, and line styles are the same as those in Fig. 2.

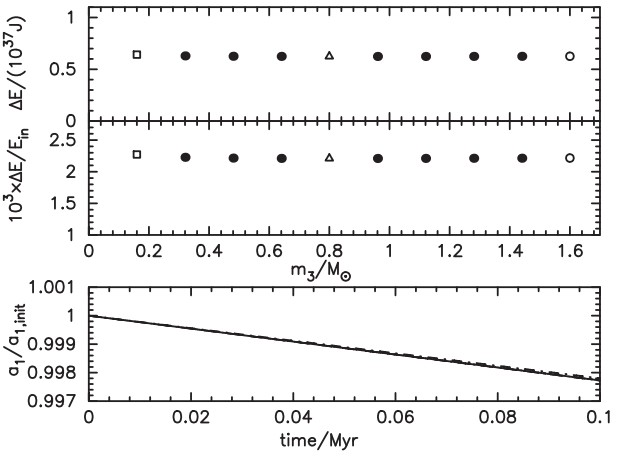

Figure 6. In this figure, the tertiary mass m_3 is varied, with all other parameters being constant and equal to the hypothetical system described in Table 1. The panels, symbols, and line styles mean the same as those in Fig. 2.

to m^2. Thus, it should not come as too much of a surprise that $\Delta E/E_{\rm in}$ is invariant with m.

3.2 Influence of the tertiary

So far, we know that, regarding the masses of the inner binary, only their relative mass ratio is important to $\Delta E/E_{\rm in}$. But what about the tertiary? Varying m_3 while keeping all other parameters constant, we arrive at Fig. 6, where it can be seen that m_3 hardly matters at all. This is probably due to the fact that the amount of energy carried in the tidal bulges on the tertiary is invariant with the mass of the tertiary – under the approximation of small tidal bulges, given the same amount of tidal force, the height of the bulges is inversely proportional to the local surface gravitational acceleration (g) of the tertiary, whereas the amount of gravitational potential energy stored per unit height of the bulge is proportional to g.

If equation (3) is to be believed, ΔE ought to scale proportionately to R_3^5 for 100 per cent dissipation efficiency. However, since we do not know how the tertiary tidal dissipation efficiency scales with

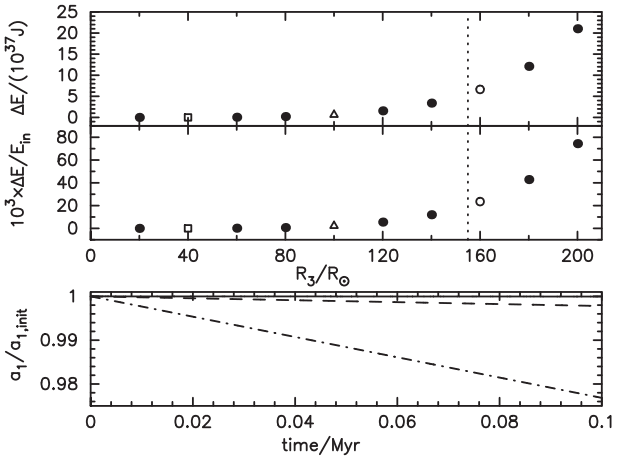

Figure 7. Here, the tertiary radius R_3, which we know to be a very influential factor in determining orbital shrinkage rate, is varied. The panels, symbols, and line styles mean the same as those in Fig. 2. Note that m_3 fills its Roche lobe in between $R_3 = 140$ and 160 $R_\odot$ (approximate value indicated by vertical dotted line), so the dash–dotted line is a generous upper limit of how fast TTs can shrink the inner binary orbit in this system without encountering Roche lobe overflow (RLOF).

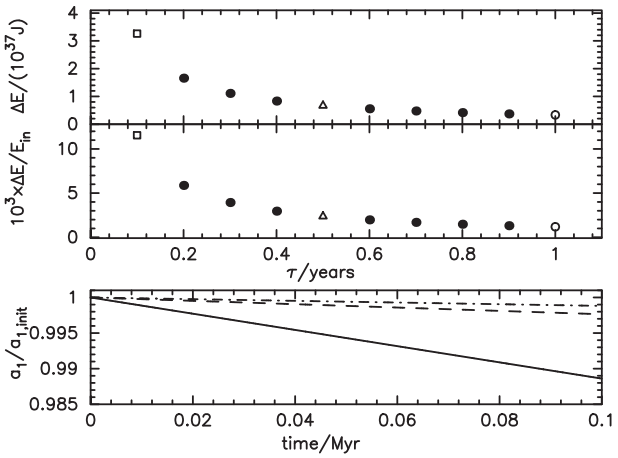

Figure 8. Varying the viscoelastic relaxation parameter τ, we arrive at this plot. The panels, symbols, and line styles mean the same as those in Fig. 2.

R_3, it is still worthwhile to calculate how $\Delta E/E_{\rm in}$ evolves with R_3. We plot this function for future fitting in Fig. 7, where we see that the influence of R_3 is indeed very great.

Finally, we vary the viscoelastic relaxation parameter τ while keeping the other parameters constant, arriving at Fig. 8.

3.3 Influence of the orbital separations

Regarding the influence of the orbital separations on $\Delta E/E_{\rm in}$, one can easily surmise from equation (3) that it is very great. Plotting how the latter responds to a change in the former in Figs 9 and 10, one can see that this is again the case.

For a_1, one can see that the larger its value, the stronger the effects of TTs. This is largely due to the binary quadrupole moment being larger with increasing a_1. However, it should be cautioned that too large an a_1 can potentially drive the triple system to instability (e.g. Eggleton & Kiseleva 1995; Mardling & Aarseth 2001). Conversely,

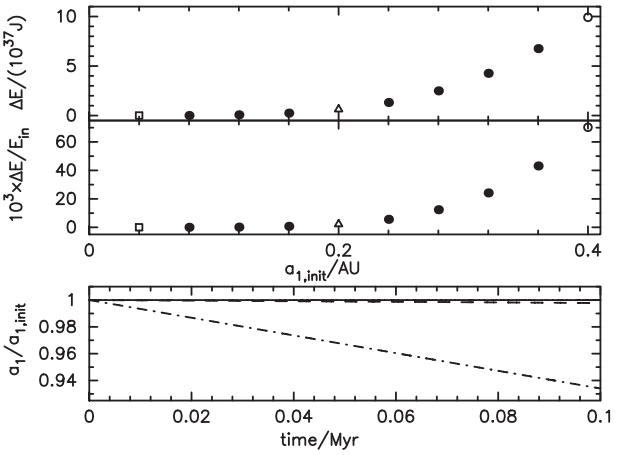

Figure 9. Similar to previous plots, only this time the initial value of the inner binary orbital separation a_1 is varied. The panels, symbols, and line styles mean the same as those in Fig. 2.

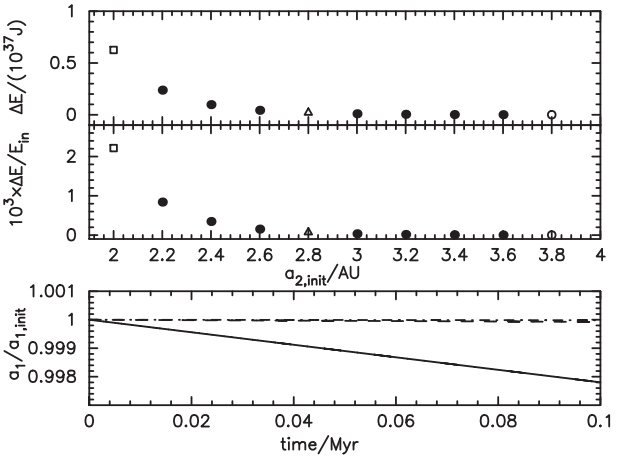

Figure 10. The outer binary separation a_2 is varied in this figure. The panels, symbols, and line styles mean the same as those in Fig. 2.

the inner orbital shrinkage stalls once a_1 is too small, as once this happens, the change in the gravitational potential of the inner binary induced by its orbital motion vanishes.

As for a_2, one would expect that, as with all tidal phenomena, tidal effects vanish quickly with increasing distance between the body undergoing tidal distortion and the rest of the system.

Throughout the plots displayed up to this point, it should be noted that the error levels are too small to warrant the addition of error bars to these plots. This will be demonstrated in the course of fitting our desired empirical function, which we proceed to do below.

3.4 Empirical function fits

To obtain the empirical function that is the final goal of this work, we assume that, over 10^5 yr,

$$\begin{aligned}\Delta E/E_{\rm in} &= f\,(q,\,R_3,\,a_1,\,a_2,\,\tau)\\ &= f_1\,(q)\,f_2\,(R_3)\,f_3\,(a_1)\,f_4\,(a_2)\,f_5\,(\tau)\,.\end{aligned} \tag{4}$$

Note that, here, we have already taken advantage of our knowledge that q is the only factor by which the masses influence the inner

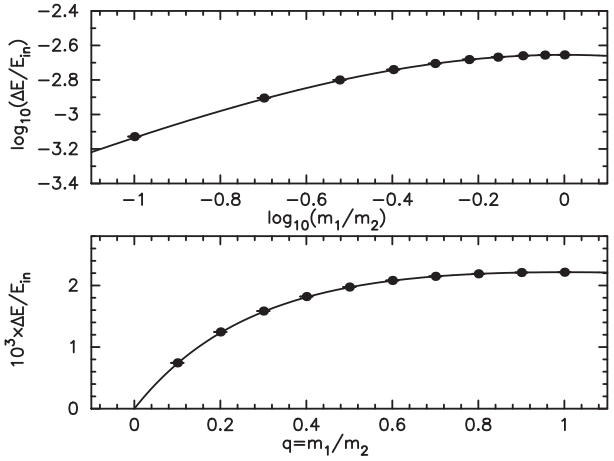

Figure 11. Weighted least-squares fit to $f_1 = 4q/(1+q)^2$. The upper panel plots the fit in log–log form, while the lower panel plots the fit in linear form. The almost invisible error bars were calculated assuming a 2×10^{33} J discrepancy in ΔE both ways.

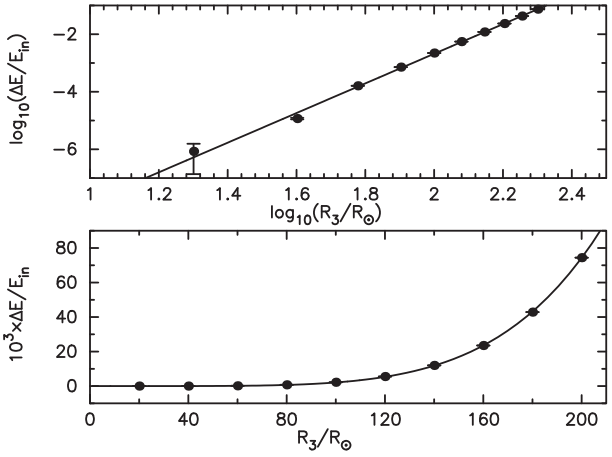

Figure 12. Least-squares weighted fit to $f_2 = A_2 R_3^{C_2}$, with weights applied according to equation (6). It was found that $C_2 = 5.2$. The upper and lower panels are the same plot in linear space and logarithmic space, respectively. Error bars are plotted for both panels, but are not easily visible in the lower panel.

binary orbital shrinkage. After much experimentation, we find that

$$f_1 = q\left(\frac{1+q}{2}\right)^{-2} = \frac{4q}{(1+q)^2} \tag{5}$$

yields the most sensible fit for f_1. This probably has a physical explanation, in that the binary quadrupole moment is the factor that drives TTs. The results of the fit are displayed in Fig. 11.

As for f_2, f_3, f_4, and f_5, we expect these functions to follow some sort of power law, and therefore we plot the data for these fits in logarithmic space, and perform linear fits to these data points using a least-squares algorithm. Attention should be paid here to the fact that our previous error estimates of 2×10^{33} J, while negligible in linear space, can be significant in logarithmic space, and therefore we calculate the error bars in logarithmic space for each data point, and weight each point by a factor of

$$w = \left[\log_{10}(\Delta E + \sigma) - \log_{10}(\Delta E - \sigma)\right]^{-2} \tag{6}$$

when applying the fitting, where σ is the error value of 2×10^{33} J we previously determined. The effect of adding this weighting to our least-squares approach is equivalent to applying a χ^2 fit. The optimum power-law indices for $f_2(R_3)$, $f_3(a_1)$, $f_4(a_2)$, and $f_5(\tau)$ are found to be 5.2, 4.8, −10.2, and −1.0, respectively, and the fitting functions considered to be optimal are displayed in Figs 12–15. These results are listed in Table 2. In general, R_3 and τ yield robust fits, whereas those for a_1 and a_2 are a little bit more suspicious towards the low energy extraction end, hinting that there is more to the story than a simple power law. However, since low values of $\Delta E/E_{\rm in}$ translates into a negligible TT effect, this should not be too much of an issue when applying our fits with a view to simulating the effects of TTs in a stellar evolution algorithm.

It should be noted here that these results invariably deviate from the values found in equation (3), for a variety of reasons. For $f_2(R_3)$, it is probably due to the fact that equation (3) was derived under the assumption of small tidal distortions in m_3, an assumption that no longer holds when R_3 is very large. Also prominent is the issue that τ is very probably intrinsically coupled with the other three in some way, which also explains the discrepancy in the indices for a_1 and a_2. Lastly, equation (3) was derived for 1/4 of an inner binary orbit under the assumption of 100 per cent efficient dissipation, while

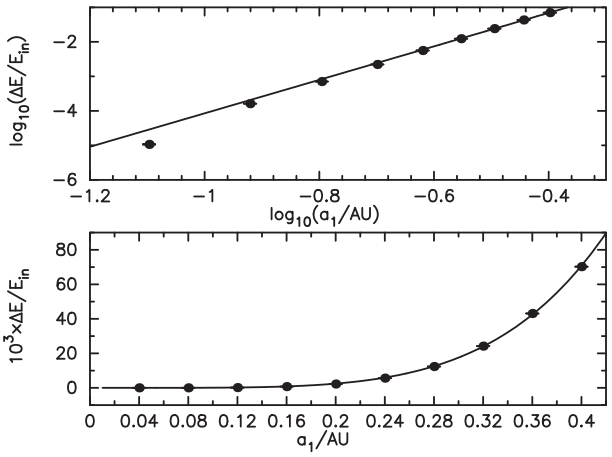

Figure 13. Least-squares weighted fit to $f_3 = A_3 a_1^{C_3}$ with weights applied according to equation (6). It was found that $C_3 = 4.8$. The upper and lower panels are the same plot in linear space and logarithmic space, respectively. Error bars are plotted for both panels, but are not easily visible in either panel.

both the orbital period and dissipation efficiency have a degree of dependence on a_1, a_2, and R_3.

Since the nature of how τ influences the viscoelastic model in our numerical model is exponential, we also attempt an exponential fit for $f_5(\tau)$, in the form of

$$f_5 = C_6\left[1 - \mathrm{e}^{-\frac{C_7}{\tau/\mathrm{yr}}}\right], \tag{7}$$

which should, in principle, collapse to $f_5 = \frac{C_6 C_7}{\tau/\mathrm{yr}}$ when $\tau/\mathrm{yr} \gg C_7$. We find that $C_6 = 0.198$ and $C_7 = 0.006$ yield the best fit, and that the fitting curve is identical in appearance to that shown in Fig. 15. Since we rarely see τ values as small as 0.006 yr, we retain our original power-law fit results for our final empirical function for simplicity, but caution our colleagues that equation (7) may be the intrinsically correct formula for τ dependence for our model. It should also be noted, however, that our model also has a discrepancy relative to the physical world, in the sense that, in the physical world, a τ value of zero would imply that the tertiary is constantly at equilibrium

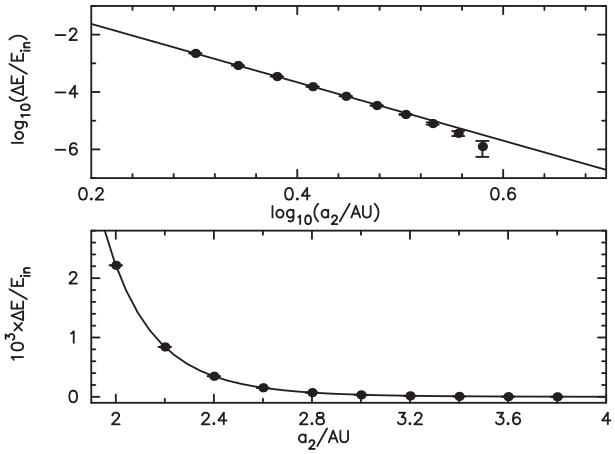

Figure 14. Least-squares weighted fit to $f_4 = A_4 a_2^{C_4}$ with weights applied according to equation (6). It was found that $C_4 = -10.2$. The upper and lower panels are the same plot in linear space and logarithmic space, respectively. Error bars are plotted for both panels, but are not easily visible in the lower panel.

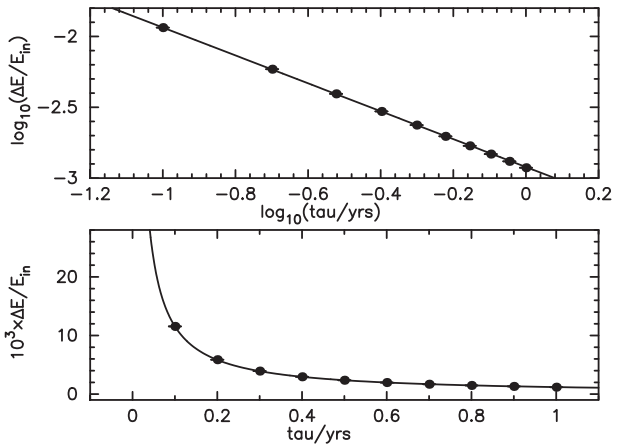

Figure 15. Least-squares weighted fit to $f_5 = A_5 \tau^{C_5}$ with weights applied according to equation (6). It was found that $C_5 = -1.0$. The upper and lower panels are the same plot in linear space and logarithmic space, respectively. Error bars are plotted for both panels, but are not easily visible in either panel.

Table 2. Results of power-law fits used to find the empirical functions $f_2(R_3)$, $f_3(a_1)$, $f_4(a_2)$, and $f_5(\tau)$.

f_X	C_X
$f_2(R_3)$	5.15
$f_3(a_1)$	4.85
$f_4(a_2)$	− 10.17
$f_5(\tau)$	− 0.98

tide, and no energy is extracted from the inner binary at all. Hence, at extremely small values of τ much shorter than the steplengths used in our simulations, any orbital shrinkage effects are merely numerical artefacts induced by our algorithm, although exactly at what τ values this is the case, it is probably extremely hard to tell without extensive real-life observations of triples undergoing TTs.

In summary, we find that $\Delta E/E_{\rm in}$ scales proportionally to $4q\,(1+q)^{-2}\,R_3^{5.2} a_1^{4.8} a_2^{-10.2} \tau^{-1.0}$ for a fixed simulation time of 10^5 yr. Since $\Delta E/E_{\rm in} = 2.22 \times 10^{-3}$ for our hypothetical scenario, and noting that the inner binary orbital shrinkage behaves linearly on time-scales of 10^5 yr, we can write this as

$$\frac{1}{a_1}\frac{{\rm d}a_1}{{\rm d}t} = \left(2.22\times10^{-8}\,{\rm yr}^{-1}\right)\frac{4q}{(1+q)^2}\left(\frac{R_3}{100\,{\rm R}_\odot}\right)^{5.2} \times \left(\frac{a_1}{0.2\,{\rm au}}\right)^{4.8}\left(\frac{a_2}{2\,{\rm au}}\right)^{-10.2}\left(\frac{\tau}{0.534\,{\rm yr}}\right)^{-1.0}. \quad (8)$$

4 DISCUSSION

Before we rush to the conclusion that our empirical function $(1/a_1)({\rm d}a_1/{\rm d}t) = (2.22 \times 10^{-8}\ {\rm yr}^{-1})\ 4q(1+q)^{-2}\ (R_3/100\ {\rm R}_\odot)^{5.2}\ (a_1/0.2\ {\rm au})^{4.8}\ (a_2/2\ {\rm au})^{-10.2}\ (\tau/0.534\ {\rm yr})^{-1.0}$ can approximate the effect of TT energy extraction rates, we should note that our simulations do not account for any correlation terms between the parameters varied. In other words, varying two different parameters at the same time may result in behaviour that deviates from what we expect when varying them one at a time. Also, it should be noted that extrapolating to parameter regimes beyond what has been simulated may also be questionable, since our fits already hint at a deviation from the power laws that we use to fit our results as we go to such regimes. For these reasons, it would be wise to conduct a few tests by comparing extrapolations of this empirical function with simulations of triple systems with parameters different to those simulated throughout the course of this work.

HD 181068 ($a_1 = 4.777\ {\rm R}_\odot$, $a_2 = 90.31\ {\rm R}_\odot$, $e_1 = e_2 = i = 0$, $m_1 = 0.870\ {\rm M}_\odot$, $m_2 = 0.915\ {\rm M}_\odot$, $m_3 = 3.0\ {\rm M}_\odot$, $R_3 = 12.46\ {\rm M}_\odot$, $\tau = 0.88$ yr) is a triple system that can be used to perform such a test, since some of its parameters lie beyond the range of our simulations in this paper. For HD 181068, we find that $\Delta E/E_{\rm in} = 5.72 \times 10^{-6}$ over 10^5 yr using our empirical function, while a full viscoelastic simulation yields $\Delta E/E_{\rm in} = 3.31 \times 10^{-6}$ over 10^5 yr. Thus, we can see that there is a significant deviation, but that the function is still accurate to within an order of magnitude.

To check for correlation terms between the parameters, we conduct a set of simulations, the details of which are listed in Table 3. All the parameters not displayed in the table are identical to those of the hypothetical scenario in Table 1. As we can see from the simulation results, our empirical function performs admirably in predicting $\Delta E/E_{\rm in}$ for these test runs.

As a further test of our empirical function, we set (a_1/a_2) to a fixed value of 0.1, and then vary a_1 to see how $\Delta E/E_{\rm in}$ evolves with changing a_1. If the our empirical function were a physical law, then since

$$\Delta E/E_{\rm in} \propto a_1^{4.8} a_2^{-10.2}, \quad (9)$$

one would expect that, with (a_1/a_2) being a constant, $\Delta E/E_{\rm in}$ should scale as a_1 to the power of −5.4. The power-law index that results from our fits is −5.0. While not fatal to the validity of our empirical function, this discrepancy implies that there is more to this relation than meets the eye. Coincidentally, an index of −5.0 is the exact power law one would expect if one were to equate ΔE with the right-hand side of equation (3), and substitute $E_{\rm in}$ using equation (1). However, since the relation between ΔE and the right-hand side of equation (3) is a complicated one, we have no reason to believe that a power law of −5.0 is intrinsic to this relation. Perhaps future studies that improve our understanding of the correlation between τ and the other orbital parameters may shed more light on this issue.

It should also be drawn to the attention of the reader that our model also suffers from the uncertainty that the second Love number, k_2, is

Table 3. Comparison between empirical function fits and corresponding results of full simulations for 10^5 yr for a set of arbitrarily selected test runs. It can be seen that the errors are relatively small, and that the performance of our empirical function is satisfactory.

Test #	m_1 ($M_\odot$)	m_2 ($M_\odot$)	m_3 ($M_\odot$)	$q(=m_1/m_2)$	a_1 (au)	a_2 (au)	R_3 ($R_\odot$)	τ (yr)	Simulated $\Delta E/E_{\rm in}$	Function $\Delta E/E_{\rm in}$
1	0.12	1.21	1.7	0.099	0.16	2.1	84	0.4	7.688×10^{-5}	8.170×10^{-5}
2	0.24	1.22	1.8	0.197	0.17	2.2	88	0.5	1.116×10^{-4}	1.160×10^{-4}
3	0.36	1.23	1.9	0.293	0.18	2.3	92	0.6	1.264×10^{-4}	1.298×10^{-4}
4	0.48	1.24	2.0	0.387	0.19	2.4	96	0.7	1.316×10^{-4}	1.340×10^{-4}
5	0.60	1.25	2.1	0.480	0.20	2.5	100	0.8	1.318×10^{-4}	1.331×10^{-4}
6	0.72	1.26	2.2	0.571	0.21	2.6	104	0.9	1.300×10^{-4}	1.298×10^{-4}
7	0.84	1.27	2.3	0.661	0.22	2.7	108	1.0	1.271×10^{-4}	1.252×10^{-4}
8	0.96	1.28	2.4	0.750	0.23	2.8	112	1.1	1.219×10^{-4}	1.201×10^{-4}
9	1.08	1.29	2.5	0.837	0.24	2.9	116	1.2	1.175×10^{-4}	1.147×10^{-4}
10	1.20	1.30	2.6	0.923	0.25	3.0	120	1.3	1.134×10^{-4}	1.094×10^{-4}

difficult to determine for most stars. In our simulations, we used $k_2 = 0.2$, which is what GCEH18 used, as prescribed by Yip & Leung (2017) for red giants, but actual values of k_2 can vary (see e.g. the value for a real red giant in Borkovits et al. 2013). However, since tidal effects, including $\Delta E/E_{\rm in}$, scale proportionally with k_2, we do not expect this to be too great an issue.

Given our results, how reliably can we expect to incorporate the effect of TTs into stellar evolution codes? As of yet, τ is still a free parameter in our empirical function fits, subject to further studies that should be aimed at breaking the degeneracy between this parameter and the other orbital parameters. Before these studies are conducted, we expect work that makes use of our current implementation of the fitting function to have an element of arbitrariness to it. However, given the possibility of calibrating this free parameter using other means such as observations, even the current form of our fitting function may have its uses. Of greater inconvenience is the fact that our empirical fitting function can only, as of yet, deal with coplanar, circular orbits. However, studies of TTs in non-coplanar, non-circular orbits would entail disentanglement from other effects present in hierarchical triples, such as Lidov–Kozai resonance (e.g. Naoz 2016), an issue that is not expected to be resolved anytime soon.

ACKNOWLEDGEMENTS

We thank our colleagues, including but not limited to Alexandre Correia, Zhengwei Liu, and Rosanne Di Stefano for valuable discussion in the course of this work.

This work was jointly supported by the Natural Science Foundation of China (Grant No. 11521303), and the Science and Technology Innovation Talent Programme of Yunnan Province (Grant No. 2017HC018).

REFERENCES

Borkovits T. et al., 2013, MNRAS, 428, 1656
Correia A. C. M., Rodríguez A., 2013, ApJ, 767, 128
Correia A. C. M., Boué G., Laskar J., Rodríguez A., 2014, A&A, 571, A50
Correia A. C. M., Boué G., Laskar J., 2016, Celest. Mech. Dyn. Astron., 126, 189
Di Stefano R., 2019, Am. Astron. Soc. Meeting, #233, 414.05
Dotter A., 2016, ApJS, 222, 8
Eggleton P., Kiseleva L., 1995, ApJ, 455, 640
Eggleton P. P., Kiseleva L. G., Hut P., 1998, ApJ, 499, 853
Fuller J., Derekas A., Borkovits T., Huber D., Bedding T. R., Kiss L. L., 2013, MNRAS, 429, 2425
Gao Y., Correia A. C. M., Eggleton P. P., Han Z., 2018, MNRAS, 479, 3604 (GCEH18)
Hurley J. R., Pols O. R., Tout C. A., 2000, MNRAS, 315, 543
Hurley J. R., Tout C. A., Pols O. R., 2002, MNRAS, 329, 897
Hut P., 1981, A&A, 99, 126
Kiseleva L. G., Eggleton P. P., Mikkola S., 1998, MNRAS, 300, 292
Mardling R. A., Aarseth S. J., 2001, MNRAS, 321, 398
Naoz S., 2016, ARA&A, 54, 441
Toonen S., Hamers A., Portegies Zwart S., 2017, Am. Astron. Soc. Meeting, #229, 326.05
Yip K. L. S., Leung P. T., 2017, MNRAS, 472, 4965

This paper has been typeset from a TEX/LATEX file prepared by the author.